Dalton
www.rsc.org/dalton

Diversity of the coordination modes of Croconate Violet. Crystal structures, spectroscopic characterization and redox studies of mono-, di- and poly-nuclear iron(II) complexes †

Brigitte Soula,[a] Anne Marie Galibert,[a] Bruno Donnadieu[b] and Paul-Louis Fabre*[a]

[a] *Laboratoire de Chimie Inorganique, EA 807, Université Paul Sabatier, 118 route de Narbonne, 31062 Toulouse, France. E-mail: fabre@chimie.ups-tlse.fr*

[b] *Laboratoire de Chimie de Coordination, UPR CNRS 8241, 205 route de Narbonne, 31077 Toulouse, France*

Received 23rd January 2003, Accepted 10th April 2003
First published as an Advance Article on the web 7th May 2003

The crystal structures of three iron(II) complexes with Croconate Violet [3,5-bis(dicyanomethylene)cyclopentane-1,2,4-trionate dianion = L^{2-}] have been determined: $K_2[FeL_2(H_2O)_4]$ **1**, $\{[Fe(2,2'\text{-bipy})L(H_2O)_2]\cdot H_2O\}_2$ **2** and $\{[FeL(H_2O)_2]\cdot 2H_2O\}_n$ **3**. Complex **1** consists of dianionic pseudo-octahedral mononuclear entities containing two N-mono-coordinated ligands in *trans* positions. Complex **2** consists of dimeric entities with metal atoms bridged by two N-coordinated Croconate Violet ligands. Complex **3** has a polymeric structure with both N- and O-coordinated Croconate Violet ligands: each iron(II) atom is bonded to three different Croconate Violet dianions and each ligand bonds three metal atoms. The magnetic properties have been investigated in the 2–300 K temperature range for complexes **2** and **3**. Magnetic susceptibility measurements for these two complexes show the presence of a long distance magnetic coupling (ferromagnetic coupling in **2** with $J = +0.18$ cm^{-1} and antiferromagnetic coupling in **3** with $J = -0.19$ cm^{-1}). The redox properties of the three complexes in dmf solution are compared to those of the free ligand.

Conjugated polynitriles such as TCNE (tetracyanoethylene) or TCNQ (7,7,8,8-tetracyano-*p*-quinodimethane) have attracted considerable attention due to their extremely high electron affinity and their delocalized π systems which allows π–π interactions. Therefore, in recent years, increasing attention has been given to the compounds obtained by reaction of these molecules with inorganic or organometallic complexes. Many of these compounds display interesting physical properties, such as highly anisotropic conductivities associated with partial charge transfer and/or partial oxidation number of the metal (molecular metals)[1] and unusual magnetic metal–metal interactions (molecular ferromagnets).[2] Several derivatives have been obtained by reaction between TCNQ and iron compounds.[3,4] In TCNQ salts, like planar molecules stack to form segregated columns and stabilization of the electronic system induces one-dimensional conductors. Otherwise, compounds containing Fe–TCNQ σ bonds as $[Fe(CH_3OH)_4(TCNQ)_2](TCNQ)$ and $[Fe(abpt)_2(TCNQ)_2]$[4] (abpt = 4-amino-3,5-bis(pyridin-2-yl)-1,2,4-triazole) exhibit interesting magnetic properties.

Croconate Violets [3,5-bis(dicyanomethylene)cyclopentane-1,2,3-trionate salts] and Croconate Blues [2,4,5-tris(dicyanomethylene)cyclopentane-1,3-dionate salts][5–9] have already attracted attention due to their reversible electrochemical behaviour,[10,11] their intense colours and some typical semiconductor properties, as a consequence of their extended π electronic systems.[12,13] Croconate Violet is, like TCNQ, essentially planar, which allows π–π interactions and a charge transfer complex has been obtained by reaction of a dicyanomethylene croconate ester with pyrene.[14]

A large number of coordination complexes have been obtained with the croconate dianion ($C_5O_5^{2-}$).[15–21] Among these complexes, the chain compound $[Fe^{II}(C_5O_5)\cdot 3H_2O]_n$[19] has been characterized. We have previously reported on the first complexes obtained using Croconate Violet (L^{2-}) as ligand:

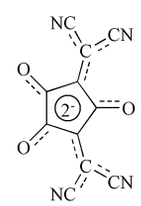

Croconate Violet or L^{2-}

$K_2[ML_2(H_2O)_2]\cdot 2H_2O$ (M = Co, Cu) and $(NBu_4)_4[CuL_3]\cdot 0.5H_2O$.[21,22] In these products, Croconate Violet acts as a chelating ligand through the two adjacent oxygen atoms as in croconate complexes. However, it is noteworthy that, in dicyanomethylene squarate ($sq^{2-} = C_4O_4^{2-}$) complexes,[23] the ligand is always coordinated by the nitrile groups.

In this paper, we report on the synthesis, crystal structures and physico-chemical characterization of three iron(II) complexes of Croconate Violet. While copper and cobalt complexes were isostructural monomers,[21,22] Croconate Violet showed, with iron(II), new coordination modes.

Experimental

Reactants and methods

All solvents and chemicals were reagent grade or better and used as received unless otherwise noted. The potassium salt of Croconate Violet ($K_2L\cdot 2H_2O$) was prepared according to the procedure described by Fatiadi and co-workers.[5–8] IR data for $K_2L\cdot 2H_2O$ (KBr, cm^{-1}): 2216w, 2198s, 2007w, 1675s, 1632w, 1616s, 1573s, 1522s, 1447s. These values agree with those previously published.[5] UV–VIS data for $K_2L\cdot 2H_2O$: λ_{max}/nm (dmf) 549 (ε/dm^3 mol^{-1} cm^{-1} 99600), 542 (sh) (95600), 429 (10600), 359 (4200).

The complexes are soluble in dmf even if, as shown by conductivity measurements, complexes **2** and **3** are partially dissociated in this solvent. The UV–VIS spectrum of **1** was measured in dmf solution on a Cary 1E spectrophotometer. Magnetic susceptibility measurements, at 300 K for **1** and in the 2–300 K temperature range for **2** and **3**, were collected for

† Electronic supplementary information (ESI) available: Table S1, hydrogen bonding interactions in the complexes. See http://www.rsc.org/suppdata/dt/b3/b300960m/

DOI: 10.1039/b300960m

powdered samples using a SQUID-based sample magnetometer on a QUANTUM Design Model MPMS instrument. $HgCo(NCS)_4$ was used as a calibrant (susceptibility at 20 °C, 16.44×10^{-6} cm^3 mol^{-1}). The molar susceptibilities were corrected for diamagnetism using Pascal's constants. The corrections were estimated at -271×10^{-6}, -245×10^{-6} and -153×10^{-6} cm^3 mol^{-1} for all the atoms of **1**, **2** and **3**, respectively. ESR spectra were recorded at ambiant temperature on crystals on a 9 GHz Bruker (ESP300E) instrument.

Electrochemical measurements were carried out at room temperature with a home-made potentiostat controlled by a PC computer. The electrochemical cell (10 cm^3) was a conventional one with three electrodes: working electrodes, platinum Pt (diameter 2 mm, EDI Tacussel) for rotating disk electrode experiments (LSV, linear sweep voltammetry), Pt (disk diameter: 0.5 mm and 50 μm) for cyclic voltammetry experiments (CV); counter electrode, Pt wire; and reference electrode, double junction SCE. The potential of the ferrocenium ion/ferrocene couple is 0.486 V *vs.* this reference[24] or 0.400 V *vs.* the standard hydrogen electrode SHE.[25] The experiments were carried out in dmf–0.1 M Bu_4NPF_6 under argon atmosphere; dmf (Acros, spectrosol) and Bu_4NPF_6 (Fluka, electrochemical grade) were used without further purification. The cyclic voltammetry was performed with the ohmic drop correction by positive feedback. The ohmic term R_u (uncompensated resistance) was first determinated by the current interrupt method.[26]

Syntheses

$K_2[FeL_2(H_2O)_4]$ 1. $FeCl_2 \cdot 4H_2O$ (66 mg, 0.333 mmol in 50 mL of water) was added to an aqueous solution of $K_2L \cdot 2H_2O$ (350 mg, 1 mmol in 120 mL). After four days at room temperature, blue-green flakes were obtained from this red solution. They were filtered off, washed with ethanol and then with diethyl ether (0.198 g, yield 88%). Found: C, 39.32; H, 1.05; N, 16.19. Calc. for $C_{22}H_8N_8O_{10}FeK_2$: C, 38.93; H, 1.18; N, 16.51%. IR data (KBr, cm^{-1}): 2236s, 2210vs (deconvolution to 2214s, 2210s and 2200w), 1680m, 1601s, 1591s, 1517s, 1484s, 1462s. UV–VIS: λ_{max}/nm (dmf) 1418 (ε/dm^3 mol^{-1} cm^{-1} 13), 1012 (48), 548 (175700), 541 (sh) (167800), 428 (20600), 358 (7800).

The same compound can be obtained from $Fe(NO_3)_3 \cdot 9H_2O$ instead of ferrous chloride: this underlines the reducing character of Croconate Violet towards iron(III).

$\{[Fe(2,2'\text{-bipy})L(H_2O)_2] \cdot H_2O\}_2$ 2. An ethanolic solution of 2,2′-bipy (78 mg, 0.5 mmol in 5 mL) was added to $Fe(NO_3)_3 \cdot 9H_2O$ (202 mg, 0.5 mmol in 100 mL of water). The orange solution was stirred for 1 h and then an aqueous solution of $K_2L \cdot 2H_2O$ (350 mg, 1 mmol in 200 mL) added. 160 mg of a violet precipitate was filtered off. After slow evaporation of the filtrate at room temperature, green monocrystals were obtained. Recrystallisation of the precipitate in water gave the same green crystals. Found: C, 49.87; H, 2.69; N, 16.31. Calc. for $C_{21}H_{14}N_6O_6Fe$: C, 50.22; H, 2.81; N, 16.73%. IR data (KBr, cm^{-1}): 2230s (br), 2204vs, 2198vs, 2186m, 2180s, 1679s, 1646w, 1620w, 1603w, 1593w, 1578s, 1562w, 1531s, 1489w, 1476w, 1442s.

$\{[FeL(H_2O)_2] \cdot 2H_2O\}_n$ 3. $K_2L \cdot 2H_2O$ (175 mg, 0.5 mmol in 150 mL of water) was added to an aqueous solution of $FeCl_2 \cdot 4H_2O$ (990 mg, 5 mmol in 50 mL). A light precipitate was filtered off and after one week, blue monocrystals were obtained from the remaining solution which were isolated and dried *in vacuo*. Found: C, 36.30; H, 1.93; N, 15.00. Calc. for $C_{11}H_8N_4O_7Fe$: C, 36.29; H, 2.22; N, 15.39%. IR data (KBr, cm^{-1}): 2228 (sh), 2213s, 1604s, 1573w, 1487s, 1459s, 1441s.

Crystallography

Data were collected at 293 K for **1**, 160 K for **2** and 180 K for **3** on a Stoe Imaging Plate Diffraction System (IPDS) diffractometer[27] equipped with an Oxford cooler cryosystems device, using graphite monochromated Mo-Kα radiation (λ = 0.71073 Å). For the three complexes, the data were collected with a crystal-to-detector distance of 70 mm, in the 2θ range 3.3–52.1° with a φ oscillation movement (φ = 0.0–200.2°, $\Delta\varphi$ = 1.3° for **1** and **2** and φ = 0.0–249.6°, $\Delta\varphi$ = 1.3° for **3**). The structures were solved by direct methods (SIR 92)[28] and refined by full-matrix least-squares procedures on F^2 (SHELXL 97)[29] included in the package WINGX 32.[30] All hydrogen atoms were located on a difference Fourier map, but they were introduced in calculations in idealized positions with an isotropic thermal parameter U_{iso} fixed at 20% higher than those of the connected atoms. All non-hydrogen atoms were anisotropically refined. Atomic scattering factors and anomalous dispersion terms were taken from the standard compilation.[31] Using the program ZORTEP,[32] drawings of molecules were plotted with 50% probability displacement ellipsoids for non-hydrogen atoms.

Crystal data, intensity measurements and structure refinement for **1**, **2** and **3** are summarized in Table 1. Selected bond lengths and angles are given in Tables 2, 3 and 4 for complexes **1**, **2** and **3**, respectively.

CCDC reference numbers 203378–203380.

See http://www.rsc.org/suppdata/dt/b3/b300960m/ for crystallographic data in CIF or other electronic format.

Results and discussion

From the reaction of iron(II) with the oxocarbon $C_5O_5^{2-}$, the complex $[Fe^{II}(C_5O_5) \cdot 3H_2O]_n$[19] is obtained: it consists of infinite chains with each metal atom coordinated to two adjacent oxygen atoms of one croconate ring and to a single oxygen of a second croconate ring. Iron(II) complexes of TCNQ as $[Fe(CH_3OH)_4(TCNQ)_2](TCNQ)$ or $[Fe(abpt)_2(TCNQ)_2]$[4] are mononuclear complexes, the octahedral environment around the metal atom containing two nitrile nitrogen atoms in *trans* positions.

Croconate Violet can coordinate to a metal centre *via* the carbocyclic π system or by the nitrile nitrogen lone pair, like unsaturated polynitriles, but also *via* the carbonyl oxygen atoms. Thus, reaction of a metal with this multidentate pseudo-oxocarbon ligand may afford various complexes.

Crystal structure of $K_2[FeL_2(H_2O)_4]$ 1

Iron(II) Croconate Violet consists of discrete mononuclear dianions $[FeL_2(H_2O)_4]^{2-}$, each associated with two potassium cations. A plot of the structure of **1** is presented in Fig. 1. Complex **1** presents the same formula, *i.e.* $K_2ML_2(H_2O)_4$, as the cobalt and copper(II) complexes we have previously described.[21,22] However, the coordination mode is different: the two

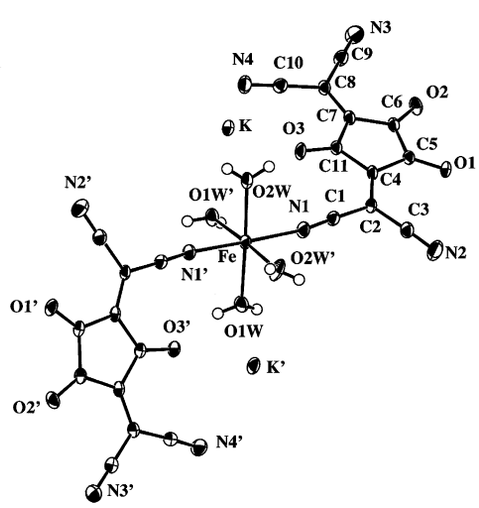

Fig. 1 Molecular structure and atom numbering scheme for $K_2[FeL_2(H_2O)_4]$ **1**.

Table 1 Summary of crystal data, intensity measurements and structure refinement for $K_2[FeL_2(H_2O)_4]$ **1**, $\{[Fe(2,2'\text{-bipy})L(H_2O)_2]\cdot H_2O\}_2$ **2** and $\{[FeL(H_2O)_2]\cdot 2H_2O\}_n$ **3**

Compound	**1**	**2**	**3**
Formula	$C_{22}H_8N_8O_{10}FeK_2$	$C_{21}H_{14}N_6O_6Fe$	$C_{11}H_8N_4O_7Fe$
M	678.41	502.23	364.06
Colour	Blue–Green	Dark green	Black
Crystal form	Plate	Plate	Parallelepiped
Crystal size/mm	0.40 × 0.35 × 0.10	0.50 × 0.30 × 0.15	0.75 × 0.50 × 0.37
Crystal system, space group	Monoclinic, $P2/n$	Triclinic, $P\bar{1}$	Triclinic, $P\bar{1}$
a/Å	9.3903(9)	10.540(7)	6.9599(8)
b/Å	6.9968(5)	10.754(8)	10.917(2)
c/Å	19.461(2)	10.977(9)	11.235(2)
α/°	—	84.22(9)	108.53(2)
β/°	92.82(2)	63.69(8)	101.44(2)
γ/°	—	67.82(8)	106.69(2)
U/Å^3	1277.1(2)	1029 (2)	734.9(2)
Z	2	2	2
D_c/g cm^{-3}	1.764	1.620	1.645
$F(000)$	680	512	368
T/K	293(2)	160(2)	180(2)
Scan range, 2θ/°	3.3–52.1	3.3–52.1	3.3–52.1
No. of measured reflections	9671	7381	7260
No. of independent reflections	2509	2793	2682
Goodness of fit S	1.034	1.034	1.047
Final R indices [$I > 2\sigma(I)$]	$R1 = 0.0316$	$R1 = 0.0681$	$R1 = 0.0306$
	$wR2 = 0.0845$	$wR2 = 0.1784$	$wR2 = 0.0789$

Table 2 Selected bond lengths (Å) and angles (°) for compound **1**

Fe–O1w	2.154(2)	Fe–O2w	2.083(2)	Fe–N1	2.102(2)
K–O3	2.651(2)	K–O1w[a]	2.876(2)	K–O1[b]	2.726(2)
K–O1[c]	2.840(2)	K–N4[d]	2.950(2)	K–N4	3.096(2)
K–O2w	3.132(2)	K–N2[b]	3.189(2)		
C5–O1	1.238(2)	C6–O2	1.250(2)	C11–O3	1.238(2)
N1–C1	1.145(2)	N2–C3	1.143(3)	N3–C9	1.145(3)
N4–C10	1.147(3)	C1–C2	1.411(2)	C2–C3	1.422(3)
C2–C4	1.385(3)	C4–C5	1.444(2)	C5–C6	1.480(3)
C6–C7	1.446(2)	C7–C8	1.376(3)	C8–C9	1.426(3)
C8–C10	1.432(2)	C7–C11	1.457(3)	C11–C4	1.449(2)
O1w–Fe–O1w[a]	88.39(8)	O2w–Fe–O2w[a]	95.9(2)	O1w–Fe–O2w[a]	87.83(7)
O1w–Fe–N1	91.79(6)	O2w–Fe–N1	88.41(7)	Fe–N1–C1	171.9(2)
N1–C1–C2	177.9(2)	N2–C3–C2	177.3(2)	N3–C9–C8	179.5(2)
N4–C10–C8	177.7(2)				
C1–C2–C4	121.7(2)	C3–C2–C4	123.0(2)	C2–C4–C5	126.9(2)
C2–C4–C11	124.3(2)	O1–C5–C4	128.4(2)	O1–C5–C6	125.0(2)
O2–C6–C5	125.2(2)	O2–C6–C7	126.3(2)	C9–C8–C7	121.2(2)
C10–C8–C7	122.0(2)	C8–C7–C6	126.9(2)	C8–C7–C11	125.7(2)
O3–C11–C7	125.8(2)	O3–C11–C4	125.8(2)		

Symmetry transformations used to generate equivalent atoms. [a] $-x + 3/2, y, -z + 1/2$. [b] $x + 1, y, z$. [c] $-x + 1, -y + 1, -z + 1$. [d] $-x + 2, +y, -z + 1$.

Croconate Violet dianions are coordinated in a monodentate mode by one nitrogen atom as in TCNQ complexes.[4] The iron atom is located in a special position on a twofold axis. The metal is surrounded octahedrically by four oxygen atoms from the water molecules and two nitrogen atoms from two different Croconate Violet dianions. The $[FeL_2(H_2O)_4]^{2-}$ dianion has a C_2 symmetry axis corresponding to the bisecting line of the O1w–Fe–O1w′ angle. Actually, the dianion is significantly *cis*-distorted with two Fe–Ow bonds longer than the two others (2.154(2) and 2.083(2) for Fe–O1w and Fe–O2w, respectively). Associated with this deformation, the O1w–Fe–O1w′ angle is 88.39(8)° while O2w–Fe–O2w′ is 95.9(2)°. The structure is best described as a square-pyramidal distorted octahedron with a $FeN_2O_2O_2$* chromophore. Most often, this *cis*-distortion is evidenced in copper complexes with strong chelating ligands such as acetate[33] or nitrite;[34] here, this may be associated with the presence of the potassium cation. The croconate ring including the oxygen atoms is planar and the two dicyanomethylene groups are twisted from the mean plane of the croconate ring in opposite directions, the deviations being 4.2 and 4.5°. Only one of the four nitrile groups of each Croconate Violet ligand is coordinated with σ donation, the Fe–N distance of 2.102(2) Å being comparable with that observed in σ bonded iron(II) complexes of TCNQ[4] (Fe–N1–C1 angle of 171.9(2)°). However, this bonding does not modify the C≡N bond lengths (1.143(3)–1.147(3) Å). The oxygen atoms of the croconate ring are uncoordinated and the bond lengths are typical for carbonyl groups (1.238(2) and 1.250(2) Å). Nitrogen and oxygen atoms surround the potassium cation with distances from 2.651(2) to 3.189(2) Å (Table 2).

The anions are laced together by hydrogen bonds, the water molecules forming hydrogen bonds with the uncoordinated nitrogen atoms N2 ($-x + 1, -y, -z + 1$) and N3 ($x + 1, y, z$), and with the oxygen atoms O2 ($x + 1/2, -y, z - 1/2$; $-x + 1, -y + 1, -z + 1$) of the croconate rings. Thus, the crystal packing of complex **1** show a large contribution of stacking interactions between the croconate rings with an interplanar distance of 3.3 Å.

Crystal structure of $\{[Fe(2,2'\text{-bipy})L(H_2O)_2]\cdot H_2O\}_2$ 2

The structure of **2** consists of $\{[Fe(2,2'\text{-bipy})L(H_2O)_2]_2$ centrosymmetric dinuclear units (Fig. 2) with two uncoordinated water molecules in the lattice. The packing of the dimeric units

Table 3 Selected bond lengths (Å) and angles (°) for compound **2**

Fe–O1w	2.102(5)	Fe–O2w	2.179(5)	Fe–N1	2.146(4)
Fe–N2	2.133(4)	Fe–N3	2.105(4)	Fe–N4[a]	2.111(4)
O1–C15	1.244(5)	O2–C17	1.233(6)	O3–C18	1.240(5)
N3–C11	1.140(6)	N4–C13	1.142(6)	N5–C20	1.151(6)
N6–C21	1.137(7)	C11–C12	1.425(7)	C12–C13	1.415(6)
C12–C14	1.381(7)	C14–C15	1.446(6)	C15–C16	1.456(7)
C16–C19	1.369(7)	C19–C20	1.437(7)	C19–C21	1.432(7)
C16–C17	1.473(6)	C17–C18	1.481(6)	C18–C14	1.440(6)
N1–C1	1.327(7)	N1–C5	1.361(6)	N2–C6	1.355(6)
N2–C10	1.331(6)	C1–C2	1.383(7)	C2–C3	1.383(8)
C3–C4	1.376(8)	C4–C5	1.393(7)	C5–C6	1.489(7)
C6–C7	1.386(7)	C7–C8	1.387(8)	C8–C9	1.376(7)
C9–C10	1.385(7)				
O1w–Fe–O2w	177.0(2)	O1w–Fe–N3	94.5(2)	O1w–Fe–N4[a]	91.1(2)
O1w–Fe–N1	90.5(2)	O1w–Fe–N2	92.0(2)	N1–Fe–N2	77.3(2)
N1–Fe–N3	96.8(2)	N2–Fe–N4[a]	95.8(2)	N3–Fe–N4[a]	89.9(2)
Fe–N3–C11	175.1(3)	Fe[a]–N4–C13	169.5(4)	N3–C11–C12	174.6(4)
N4–C13–C12	175.2(5)	N5–C20–C19	172.8(5)	N6–C21–C19	174.5(5)
C11–C12–C13	113.4(4)	C11–C12–C14	123.2(4)	C20–C19–C21	113.4(4)
C20–C19–C16	123.3(4)	O1–C15–C14	125.8(4)	O1–C15–C16	125.9(4)
O2–C17–C16	127.4(4)	O2–C17–C18	125.6(4)	O3–C18–C14	128.1(4)
O3–C18–C17	124.2 (4)	Fe–N1–C1	126.1(3)	Fe–N1–C5	114.8(3)
Fe–N2–C6	116.1(3)	Fe–N2–C10	125.4(3)		

Symmetry transformation used to generate equivalent atoms: [a] $-x + 2, -y, -z + 2$.

Table 4 Selected bond lengths (Å) and angles (°) for compound **3**

Fe–O1w	2.078(2)	Fe–O2w	2.083(2)	Fe–O1	2.213(2)
Fe–O2	2.176(2)	Fe–N3[a]	2.103(2)	Fe–N1[b]	2.117(2)
O1–C1	1.260(2)	O2–C2	1.241(2)	O3–C4	1.231(2)
N1–C7	1.143(2)	N2–C8	1.153(3)	N3–C10	1.149(3)
N4–C11	1.142(2)	C1–C5	1.424(3)	C1–C2	1.468(2)
C2–C3	1.444(2)	C3–C9	1.378(2)	C3–C4	1.460(3)
C4–C5	1.466(2)	C5–C6	1.386(3)	C6–C7	1.418(2)
C6–C8	1.426(3)	C9–C10	1.415(3)	C9–C11	1.436(2)
O1w–Fe–O2w	175.63(7)	O1w–Fe–O1	87.04(6)	O1w–Fe–O2	91.20(6)
O1w–Fe–N3[a]	91.68(7)	O1w–Fe–N1[b]	92.62(6)	O1–Fe–O2	78.75(5)
N1[b]–Fe–N3[a]	94.25(6)	O1–Fe–N1[b]	91.50(6)	O2–Fe–N3[a]	95.59(6)
Fe–O1–C1	107.8(2)	Fe–O2–C2	108.6(2)	Fe–N3[a]–C10[a]	174.7(2)
Fe–N1[b]–C7[b]	177.8(2)	O1–C1–C2	120.8(2)	O1–C1–C5	130.1(2)
O2–C2–C1	122.7(2)	O2–C2–C3	129.8(2)	O3–C4–C3	125.3(2)
O3–C4–C5	126.5(2)	C3–C9–C10	121.3(2)	C3–C9–C11	123.1(2)
C5–C6–C7	120.9(2)	C5–C6–C8	124.2(2)	N1–C7–C6	176.9(2)
N2–C8–C6	174.5(2)	N3–C10–C9	178.1(2)	N4–C11–C9	175.1(2)

Symmetry transformations used to generate equivalent atoms: [a] $-x + 1, -y + 2, -z$. [b] $-x + 2, -y + 2, -z + 1$.

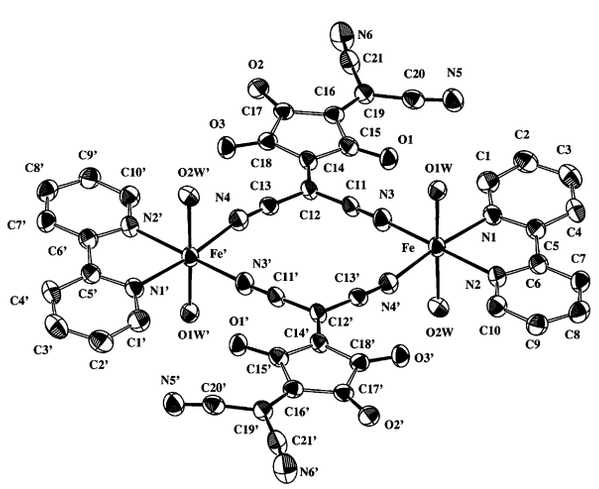

Fig. 2 Molecular structure and atom numbering scheme for {[Fe(2,2′-bipy)L$(H_2O)_2$]·H_2O}$_2$ **2**.

shows a stacking of quasi-planar molecules (except for the water molecules) with an interplanar distance of 3.6 Å. Each metal atom is surrounded octahedrically by two oxygen atoms of water molecules in opposite positions (O1w–Fe–O2w = 177.0(2) Å) and four nitrogen atoms in an equatorial plane: two of them arising from the 2,2′-bipy molecule that forms a five-membered ring with the metal and the two other arising from nitrile groups of two different Croconate Violet ligands. The Fe–N bond distances are in the range 2.105(4)–2.146(4) Å while the two Fe–Ow are shorter (Fe–O1w 2.102(5) Å) or longer (Fe–O2w 2.179(5) Å). In the equatorial plane, the N3–Fe–N4′ angle value is close to 90° (N3 and N4 arising from the two different Croconate Violet ligands) while N1–Fe–N2 is 77.3(2)° (N1 and N2 corresponding to the 2,2′-bipy molecule). Two Croconate Violet ligands bridge two iron atoms with an Fe ··· Fe distance of 7.147 Å, each ligand being bonded by the two nitrogen atoms of the same dicyanomethylene group. Such a type of coordination has been observed before in $[M(TCNQ)(TCNQ–TCNQ)_{0.5}(MeOH)_2]_n$ (M = Mn, Zn)[35] and also in $[Mn(TCNQ)_2(H_2O)_2]_n$[35] and AgTCNQ[36] polymers in which the four nitrogen atoms of TCNQ are coordinated to four different metal atoms. The Fe–N3–C11 and Fe–N4′–C13′ angles are 175.1(3) and 169.5(4)°, respectively, with σ donation from the nitrile group. The average value of the C≡N bond lengths is little affected by complexation (1.142(6) and 1.140(6) Å for the coordinated nitrile groups and 1.151(6) and 1.137(7) Å for the uncoordinated groups). The croconate ring including

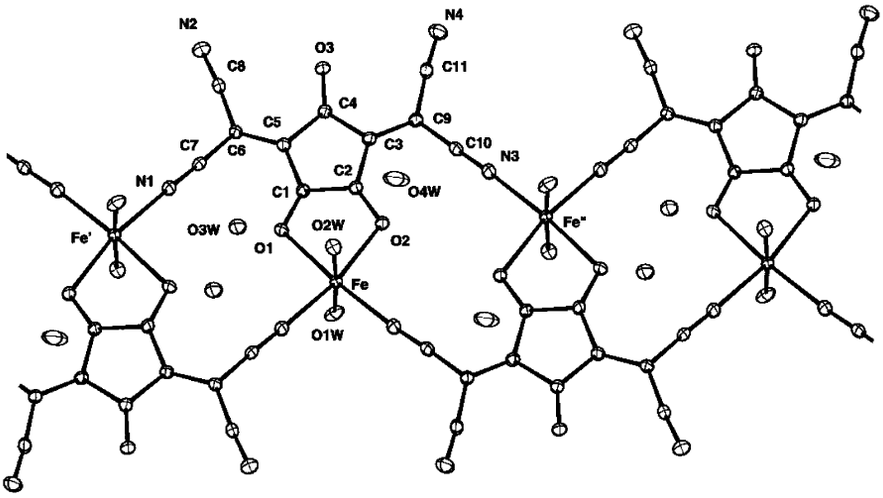

Fig. 3 Molecular structure and atom numbering scheme for $\{[FeL(H_2O)_2]\cdot 2H_2O\}_n$ **3** (symmetry transformations used to generate equivalent atoms: $'\ -x+1, -y+2, -z$. $''\ -x+2, -y+2, -z+1$).

the three oxygen atoms is planar but the dicyanomethylene groups are twisted from the ring plane in the same direction, the deviations being 5.37° for the linked group and 2.90° for the non-bonded one. As in complex **1**, the bond lengths of the uncoordinated carbonyl groups are normal.

The hydrogen bonding network in complex **2** involves the two coordinated water molecules, the water molecule of the lattice and the O1 ($-x+2, -y+1, -z+1$), O2 ($-x+1, -y, -z+2$), O3 ($x, y+1, z$), N5 ($x+1, y, z$) and N6 ($x+1, y+1, z$) atoms.

Crystal structure of $\{[FeL(H_2O)_2]\cdot 2H_2O\}_n$ 3

The crystal structure of **3** comprises an infinite chain of $[FeL(H_2O)_2]$ units oriented parallel to the [101] direction, with two uncoordinated water molecules per iron atom in the lattice. A perspective view of the polymer, along with the numbering scheme, is shown in Fig. 3. Two Fe ··· Fe distances alternately occur along the chain: Fe ··· Fe″ ($1-x, 2-y, -z$) 6.098 Å and Fe ··· Fe′ ($2-x, 2-y, 1-z$) 6.279 Å, with crystallographic inversion centres located at the middle of these distances. Each iron(II) atom is bonded to three different Croconate Violet dianions using four coordination sites: two adjacent oxygen atoms of one Croconate Violet ion (O1 and O2) and two nitrogen atoms (N1″ and N3′) from the two other Croconate Violet ions. The pseudo-octahedral geometry at the metal atom is made up by two oxygen atoms arising from two water molecules (O1w and O2w). It is of note that the chelating ligand coordinates in an asymmetrical bidentate mode, Fe–O1 and Fe–O2 being 2.213(2) and 2.176(2) Å, respectively. However, this asymmetry is much weaker than that observed in the chain complex $[Fe^{II}(C_5O_5)\cdot 3H_2O]_n$[19] (2.34 and 1.98 Å) or in the $K_2[CuL_2(H_2O)_2]$ complex (2.33 and 1.98 Å). The two Fe–N distances are of the same order (2.103(2) and 2.117(2) Å for Fe–N3′ and Fe–N1″, respectively) than evidenced in complex **1**, or in $[Fe(CH_3OH)_4(TCNQ)_2](TCNQ)$[4] (2.127(2) Å). The angles at the metal are close to 90° except for the angle at the chelating croconate ligand (O1–Fe–O2 78.75(5)°), a value quite similar to that observed in $[Fe^{II}(C_5O_5)\cdot 3H_2O]_n$.[19] In the Croconate Violet moiety, bonded to three metal atoms, each dicyanomethylene group contains one coordinated nitrogen atom (N1 or N3) and one uncoordinated atom (N2 or N4). The croconate ring including the oxygen atoms is planar but the dicyanomethylene groups are twisted from the plane in the same direction, the deviations being 11.44° for C6C7C8N1N2 and 3.56° for C9C10C11N3N4. The chelating coordination of the Croconate Violet ion to iron(II) causes the lengthening of the C1–O1 bond (1.260(2) Å) corresponding to the most coordinated oxygen atom (shortest Fe–O bond).

In the elemental unit, a hydrogen bond arises between the uncoordinated water molecule (O3w) and one of the coordinated oxygen atoms (O1). Inter-unit connections are *via* hydrogen bonds between water molecules themselves and between water molecules and the uncoordinated nitrogen atoms N2 ($x, y+1, z$) and N4 ($x+1, y+1, z+1$) or the oxygen atoms of the croconate ring O1 and O3 ($x, y-1, z$).

IR and electronic spectroscopies

The IR spectrum of Croconate Violet has been analysed by Fatiadi and co-workers.[5–8] It is essentially characterized by two bands at 2216w and 2198vs cm^{-1} attributed to ν(CN) stretching frequencies and a band at 1674m cm^{-1} attributed to the carbonyl groups. In the spectrum of **1**, two bands are observed at 2236 and 2210 cm^{-1}. The most shifted band is attributed to the coordinated nitrile group: the C–N bond strength increases upon coordination (due to the σ donation from the nitrogen lone pair of the nitrile, which has some antibonding character). Moreover, the band at 2210 cm^{-1} may be deconvoluted into three bands at 2214, 2210 and 2200 cm^{-1} showing the inequivalence of the free nitrile groups. The carbonyl vibration is, as expected, little affected by complexation and observed at 1680 cm^{-1}. The IR spectrum of **2** is quite similar to the spectrum of **1**. The ν(CN) bands are observed at 2230, 2204, 2198, 2186 and 2180 cm^{-1}, the first broad one being attributed to the coordinated cyano groups, and the others, centered at 2192 cm^{-1}, corresponding to the free nitrile groups. The characteristic carbonyl group vibration is observed at 1679 cm^{-1}. The spectrum of **3** confirms the coordination at the same time by the nitrile and the carbonyl groups. A ν(CN) band is observed at 2213 cm^{-1} with a shoulder at higher frequency (2228 cm^{-1}). These two values correspond, respectively, to the free and to the coordinated nitrile groups. The most relevant feature is the complete disappearance of the band at 1674 cm^{-1} attributed to the carbonyl groups in the free ligand. In the spectra of the cobalt and copper complexes of Croconate Violet the complete disappearance of ν(CO) has also been observed even if one of the carbonyl groups remains uncomplexed.[21,22] Due to more or less uniform electronic distribution along the bonds in the free ligand, the group of bands between 1610 and 1510 cm^{-1} are attributed to combinations of C=O, C=C and $C–C(CN)_2$ vibrations. These bands are not significantly shifted upon complexation in the three complexes.

Croconate Violet and other croconate dyes display strong absorption bands in the visible region and they have been investigated for their photo-electrochemical sensitising and electro-catalytic properties.[11–13] In dmf, these strong absorption bands (542 and 549 nm) associated with the bond-delocal-

isation structure (π–π* transitions) are not affected in complex **1**. Octahedral iron(II) complexes usually exhibit a broad $^5T_{2g} \longrightarrow {}^5E_g$ absorption band which is frequently split into two components owing to octahedral distorsion: complex **1** shows two absorptions at 1012 and 1418 nm, associated with low values of molar extinction coefficients.

Magnetic data

At 300 K, the μ_{eff} values (5.80, 5.20 and 5.29 μ_B for **1**, **2** and **3**, respectively) are higher than the spin only value (4.90 μ_B), as usually observed for Fe(II), due to the splitting of the $^5T_2$ ground state by spin–orbit coupling.

For the monomer **1**, the unexpected value of $\mu_{eff} = 5.80\ \mu_B$ for an Fe(II) complex may be explained by the presence of ferromagnetic impurities, since infinite field extrapolation gives a μ_{eff} value of 5.23 μ_B

Plots of the magnetic moment μ_{eff} per Fe, *vs.* temperature are shown in Fig. 4 for complexes **2** and **3**. In iron dimers, each Fe(II) has local spin S_1 and S_2 which, in the absence of antiferromagnetic behaviour, may be either non-interacting ($S_1 = S_2 = 2$, spin only value) or magnetically coupled to give a ground state $S = S_1 + S_2 = 4$. For complex **2**, the variation of the reciprocal molar magnetic susceptibility *vs.* temperature is described by the Curie–Weiss law: $C = 3.38\ cm^3\ K\ mol^{-1}$ and $\theta = 0.9$ K. Fig. 4 shows the increase of the magnetic moment with decreasing temperature from 5.20 μ_B at 300 K to 5.48 μ_B at 10 K. Below 10 K, the values decrease sharply, reaching 4.21 μ_B at 2 K. In the low temperatures region, the lowering of the magnetic moment may be attributed either to a significant antiferromagnetic component arising from dimer–dimer interactions, or to the presence of zero-field splitting effects on the high spin Fe(II) centres. No trace of organic radical has been evidenced by ESR measurements on crystals of **2**. Thus, the temperature dependent magnetic behaviour was modeled using the theory of Heisenberg, Dirac and Van Vleck for magnetic coupling in a dinuclear system.[37] No attempt was made to model either spin–orbit coupling or zero-field splitting phenomena. The temperature-dependent susceptibility expressions used in the simulations were those derived from the general isotropic exchange Hamiltonian, $H = -2JS_1 \cdot S_2$, where J is the intramolecular exchange interaction. The generalized expression for the magnetic susceptibility is given by the equation:

$$\chi_M = (Ng^2\beta^2/kT)[(2e^{2x} + 10e^{6x} + 28e^{12x} + 60e^{20x})/(1 + 3e^{2x} + 5e^{6x} + 7e^{12x} + 9e^{20x})]$$

where $x = J/kT$.[37] Least-squares optimisation of this equation for **2** gave $g = 2.12$ and $J = +0.18\ cm^{-1}$.

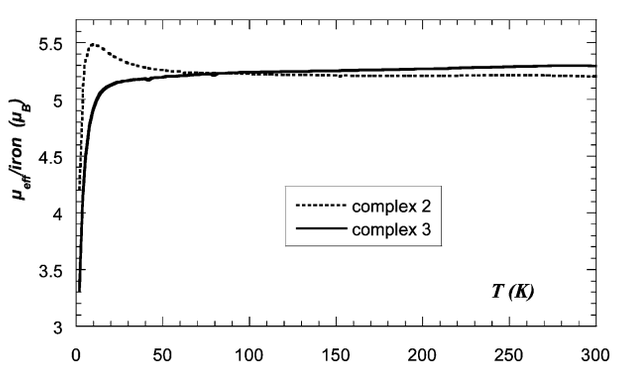

Fig. 4 Magnetic moment μ_{eff} per Fe *vs.* temperature for $\{[Fe(2,2'\text{-bipy})L(H_2O)_2]\cdot H_2O\}_2$ **2** and $\{[FeL(H_2O)_2]\cdot 2H_2O\}_n$ **3**.

The polynuclear complex **3** shows very weak antiferromagnetic coupling. The variation of the reciprocal molar magnetic susceptibility data *vs.* temperature is described by the Curie–Weiss law: $C = 3.53\ cm^3\ K\ mol^{-1}$ and $\theta = -2.5$ K. Fig. 4 shows a slow decrease of the magnetic moment with decreasing temperature from 5.29 μ_B at 300 K to 5.12 μ_B at 20 K, then a drop of the magnetic moment is observed, to reach 3.32 μ_B at 2 K. Use of an Heisenberg chain model[38] for $S = 2$, which did not contain zero field splitting terms, gave $g = 2.17$ and $J = -0.19\ cm^{-1}$.

The very weak coupling constants found for complexes **2** and **3**, (ferromagnetic coupling in **2** or antiferromagnetic coupling in **3**) are in agreement with the X-ray structural data giving large Fe ··· Fe distances in the two complexes (7.147 Å for **2** and 6.098 Å for **3**). The high effective g values allow for orbital degeneracy on Fe(II). Concerning the croconate ligand, polynuclear complexes of general formula $[M(C_5O_5)\cdot 3H_2O]$[16,19] (M = Cu(II), Mn(II), Fe(II)) exhibit weak antiferro intrachain interactions *via* the croconate dianion with $J = -0.54\ cm^{-1}$ in the iron complex. This weak coupling exchange value is attributed to the mono-/bi-dentate mode of coordination of croconate, the coupling being larger in the case of a bis-bidentate croconate bridge.[18] Complexes **2** and **3** may be also compared with complexes containing a derivative of chloroanilic acid[39] (can = 2,5-dichloro-3,6-dihydroxycyclohexa-2,5-diene-1,4-dione). This bridging ligand has a delocalised π system providing electronic communication between the metal centres: the polymeric complex $[Fe(can)(H_2O)_2]\cdot H_2O$, with an intramolecular Fe ··· Fe separation of 7.847(3) Å, displays weak intrachain ferromagnetic coupling ($J = +0.47\ cm^{-1}$). Very few examples are known of structurally identified diiron(II) compounds presenting a ferromagnetic coupling. Holm and coworkers[40] described dinuclear Schiff base species containing μ-alkoxo bridges with an Fe ··· Fe separation of 3.2 Å and $J = +1.23\ cm^{-1}$. For another μ-oxo bridge dimer with Fe ··· Fe separations of the same order, Stassinopoulos *et al.*[41] report a value of $J = +2.65\ cm^{-1}$. A ferromagnetic coupling in solution is also observed in $[(FeCl(tmen))_2(\mu\text{-}Cl)_2]$.[42]

Electrochemical study

In the electroactivity window of dmf–Bu_4NPF_6, the cyclic voltammograms of the complexes present the same shape and are compared to those of the Croconate Violet. Due to the partial dissociation of complexes **2** and **3** in dmf, only the electrochemistry of complex **1** can be fully described. As already mentioned,[10,43] the cyclic voltammogram of the free ligand (Fig. 5) shows two successive monoelectronic oxidations:

The first step ($E° = 0.42$ V) corresponds to the oxidation of the dianion into the radical-anion,

$$L^{2-} \rightleftharpoons L^{\bullet -} + e^- \quad (1)$$

The second step ($E° = 0.90$ V) corresponds to the oxidation of the radical-anion into the neutral form,

$$L^{\bullet -} \rightleftharpoons L + e^- \quad (2)$$

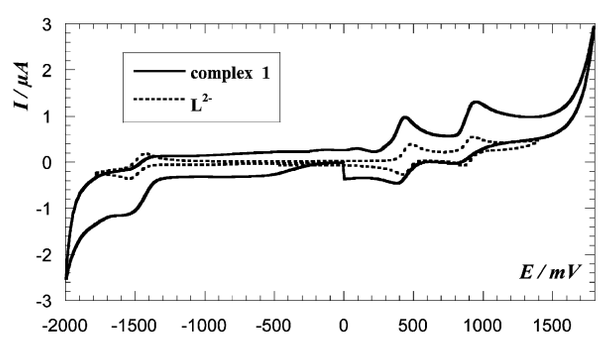

Fig. 5 Cyclic voltammograms at a Pt disk electrode (diameter 0.5 mm) in dmf–0.1 M Bu_4NPF_6, potential scan speed 0.1 V s^{-1} (starting from 0 V towards cathodic, then anodic potentials and back to 0 V): (···) L^{2-}, 1 mM; (—) complex **1**, 1 mM.

Moreover, a reduction process ($E^\circ = -1.49$ V) is observed which yields a radical-trianion:[43]

$$L^{2-} + e^- \rightleftharpoons L^{\bullet 3-} \quad (3)$$

The forward peak currents present the same hight and follow the Randles–Sevcik equation for a simple electron transfer. The electrochemical systems 1, 2 and 3 appeared reversible at the used potential scan speeds (from 0.01 up to 1000 V s^{-1}).

The cyclic voltammogram of complex **1** (Fig. 5) consists in the addition of the ligand electrochemical systems (two ligands per complex) and an irreversible reduction at −0.5 V. The signals of the ligand are little affected by complexation, but a slight displacement of the peak potentials is observed. This means that the different redox forms of the ligand are still in the coordination sphere of the iron. Moreover, the current increase reflects the stoechiometry and the diffusion coefficient of the complex. The diffusion coefficients were determined through the Levich relation by hydrodynamic voltammetry (Fig. 6) on the first oxidation process: system 1 ($L^{\bullet -}/L^{2-}$). According to the size of the species, the diffusion coefficient of complex **1** ($D = 3.6 \times 10^{-6}$ cm^2 s^{-1}) is lower than that of the free ligand ($D = 4.5 \times 10^{-6}$ cm^2 s^{-1}); this is in agreement with the non-dissociation of the complex in dmf as suggested by conductimetric measurements. The irreversible reduction at −0.5 V induces electrode fouling; as a result, system 3 is poorly defined. Taking into account the voltammograms in dmf of $FeCl_2$ or $Fe(NO_3)_3$, this reduction may be attributed to iron(II) reduction. Due to electrode fouling in the reduction domain, the following discussion is restricted to the oxidation processes. Fig. 6 shows the voltammograms at a rotating disk Pt electrode under stationary conditions. As expected for the free ligand L^{2-}, we observed two waves ($E_{1/2} = 0.42$ and 0.90 V) corresponding to the two successive monoelectronic oxidations. As for complex **1**, the two waves are still present ($E_{1/2} = 0.45$ and 0.93 V) and only slightly displaced. For the electrochemical system 1 ($L^{\bullet -}/L^{2-}$), the I_{D1} diffusion current increase is in agreement with the stoichiometry and the diffusion coefficient of the complex. On the contrary, the I_{D2} diffusion current corresponding to system 2 is much higher than expected. The ratio of the diffusion currents I_{D2}/I_{D1} for complex **1** is around 1.5. This value matches with a two-electron exchange for the first wave (two ligands, $L^{\bullet -}/L^{2-}$) and a three-electron exchange for the second wave: two ligands ($L/L^{\bullet -}$) and iron (Fe^{III}/Fe^{II}); the redox potentials of $L/L^{\bullet -}$ and Fe^{III}/Fe^{II} are of the same order of magnitude, around 0.9 V. In dmf, $Fe(NO_3)_3$ presents a reversible system at $E^\circ = 0.47$ V for the Fe^{III}/Fe^{II} transfer. The anodic potential displacement is related to the relative complex formation constants of Fe^{III} and Fe^{II} complexes:[44] Fe^{II} is much more strongly complexed than Fe^{III}, the complex formation constant of Fe^{II} being around 10^8 higher than that for Fe^{III}.

Fig. 7 shows the cyclic voltammograms at a Pt disk electrode. The free ligand L^{2-} shows two reversible systems corresponding to the two successive monoelectronic oxidations. For complex

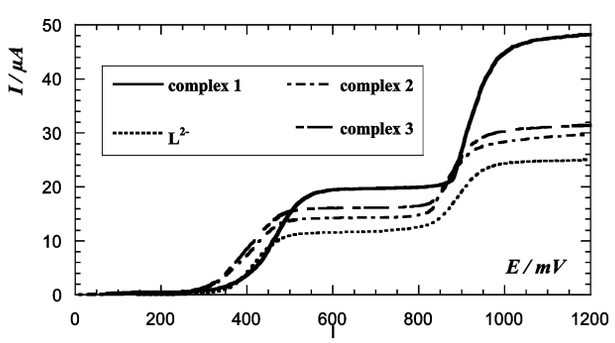

Fig. 6 Voltammograms at a Pt disk rotating electrode (diameter 2 mm, rotation speed 1000 rpm) in dmf–0.1 M Bu_4NPF_6: (···) L^{2-}, 1 mM; (—) complex **1**, 1 mM; (- - -) complex **2**, 1 mM; (- —) complex **3**, 1 mM.

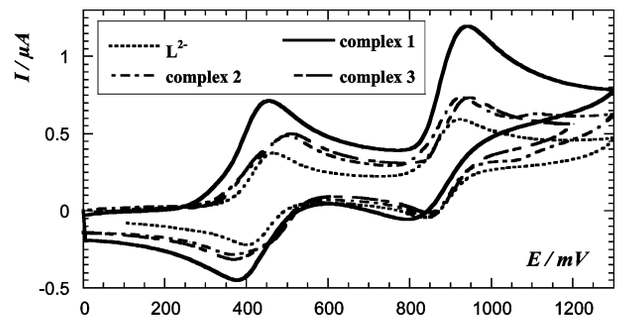

Fig. 7 Cyclic voltammograms at a Pt disk electrode (diameter 0.5 mm) in dmf–0.1 M Bu_4NPF_6, potential scan speed 0.1 V s^{-1} (starting from 0 V towards anodic potentials and back to 0 V): (···) L^{2-}, 1 mM; (—) complex **1**, 1 mM; (- - -) complex **2**, 1 mM; (- —) complex **3**, 1 mM.

1, the first electron transfer is still reversible while the second transfer (three electrons) is more or less reversible. Moreover, the I_{P2} peak current (system 2) is also higher than the I_{P1} peak current (system 1) but the ratio of the peak currents I_{P2}/I_{P1} is only 1.3 at 0.1 V s^{-1} and decreases when the potential scan speed is increased. Thus, the cyclic voltammogram of complex **1** consists of a first reversible two-electron exchange (system 1, two ligands) and in the addition of a reversible two-electron exchange (system 2, two ligands) and a slow electron transfer for Fe^{III}/Fe^{II} in the second process.

The high redox potential of Fe^{III}/Fe^{II} in complex **1** rationalizes the synthesis products. When starting with iron(III) salts, we always obtained iron(II) complexes since iron(III) is reduced by the ligand which is in agreement with the determinated redox potentials. Such a behaviour has already been observed in the synthesis of copper complexes of the 3,4-bis(dicyanomethylene)-cyclobutane-1,2-dione dianion.[23]

Figs. 6 and 7 also show the voltammograms of complexes **2** and **3**. Complex **2** is dissociated in dmf and its conductivity is typical of a 1 : 1 electrolyte while complex **3** is partially dissociated. Under stationary conditions (Fig. 6), the two waves are observed: complex **2**, $E_{1/2}$ at 0.41 and 0.87 V; complex **3**, $E_{1/2}$ at 0.40 and 0.88 V. The first wave appears distorted and the ratio of the diffusion currents I_{D2}/I_{D1} are lower than 1 (0.93 for complex **2** and 0.88 for complex **3**). Moreover, at equal concentrations (1 mM), the diffusion currents are higher than for the free ligand. According to cyclic voltammetry (Fig. 7), the first electrochemical system appears to be split into two processes for complexes **2** and **3**. The occurrence of two redox systems around 0.4 V may be explained by the dissociation of the complexes. Taking into account the redox potential of solvated Fe^{III}/Fe^{II} (0.47 V), the first peak may be due to the oxidation of the ligand and Fe^{II} formed from dissociation of the complexes. Moreover, the voltammogram of complex **2** shows a reversible couple ($E^\circ = 1.11$ V) which disappears when the potential scan speed is increased. This signal may be attributed to the oxidation of $[Fe(bipy)_3]^{2+}$ according the potential value:[45,46]

$$[Fe(bipy)_3]^{2+} \rightleftharpoons [Fe(bipy)_3]^{3+} + e^-$$

$[Fe(bipy)_3]^{2+}$ is produced at the electrode during the oxidation process. When the potential scan speed is increased the formation of $[Fe(bipy)_3]^{2+}$ is blocked.

Finally, among these complexes, complex **1** appears to be the most stable compound. However, its structure is different from the copper[21] or cobalt[22] analogs, since the ligand is here N-mono-coordinating. The two other complexes, dissociated in solution, present a N,N-bridging ligand for the dimer **2** and a N,O-coordinating ligand for the polymer **3**. This latter complex may lead to a monomer complex analogous to **1** in solution.

Acknowledgements

We thank a student A. Ali for her participation in the syntheses.

References

1 S. Hünig and P. Erk, *Adv. Mater.*, 1991, **3**, 225 and references therein.
2 J. S. Miller and A. J. Epstein, *Angew. Chem., Int. Ed. Engl.*, 1994, **33**, 385 and references therein.
3 L. Ballester, A. Gutiérrez, M. F. Perpiñán, S. Rico, M. T. Azcondo and C. Bellito, *Inorg. Chem.*, 1999, **38**, 4430; L. Ballester, A. Gutiérrez, M. F. Perpiñán, M. T. Azcondo and A. E. Sánchez, *Synth. Met.*, 2001, **120**, 965.
4 H. Oshio, E. Ino, T. Ito and Y. Maeda, *Bull. Chem. Soc. Jpn.*, 1995, **68**, 889; P. J. Kunkeler, P. J. van Koningsbruggen, J. P. Cornelissen, A. N. van der Horst, A. M. van der Kraan, A. L. Spek, J. G. Haasnoot and J. Reedijk, *J. Am. Chem. Soc.*, 1996, **118**, 2190.
5 A. J. Fatiadi, *J. Am. Chem. Soc.*, 1978, **100**, 2586.
6 A. J. Fatiadi, *Synthesis*, 1978, **3**, 165.
7 A. J. Fatiadi, *J. Org. Chem.*, 1980, **45**, 1338.
8 V. L. Himes, A. D. Mighell, C. R. Hubbard and A. J. Fatiadi, *J. Res. Natl. Bur. Stand.*, 1980, **85**, 87.
9 A. J. Fatiadi, *Oxocarbons*, Academic Press, New York, 1980.
10 L. M. Doane and A. J. Fatiadi, *J. Electroanal. Chem.*, 1982, **135**, 193.
11 P. V. Kamat and M. A. Fox, *J. Electroanal. Chem.*, 1983, **159**, 49.
12 P. V. Kamat and M. A. Fox, *Chem. Phys. Lett.*, 1982, **92**, 595.
13 P. V. Kamat, M. A. Fox and A. J. Fatiadi, *J. Am. Chem. Soc.*, 1984, **106**, 1191.
14 R. M. Doherty, J. M. Stewart, A. D. Mighell, C. R. Hubbard and A. J. Fatiadi, *Acta Crystallogr., Sect. B*, 1982, **38**, 859.
15 M. D. Glick, G. L. Downs and L. F. Dahl, *Inorg. Chem.*, 1964, **3**, 1712; M. D. Glick and L. F. Dahl, *Inorg. Chem.*, 1966, **5**, 289.
16 D. Deguenon, G. Bernardinelli, J. P. Tuchagues and P. Castan, *Inorg. Chem.*, 1990, **29**, 3031.
17 P. Castan, D. Deguenon and F. Dahan, *Acta Crystallogr.*, 1991, **47**, 2656.
18 I. Castro, J. Sletten, J. Faus, M. Julve, Y. Journaux, F. Lloret and S. Alvarez, *Inorg. Chem.*, 1992, **31**, 1889; I. Castro, J. Sletten, J. Faus and M. Julve, *J. Chem. Soc., Dalton Trans.*, 1992, 2271.
19 A. Cornia, A. C. Fabretti, A. Giusti, F. Ferraro and D. Gatteschi, *Inorg. Chim. Acta*, 1993, **212**, 87.
20 C.-C. Wang, C.-H. Yang and G.-H. Lee, *Inorg. Chem.*, 2002, **41**, 1015.
21 F. Dumestre, B. Soula, A. M. Galibert, P.-L. Fabre, G. Bernardinelli, B. Donnadieu and P. Castan, *J. Chem. Soc., Dalton Trans.*, 1998, 4131.
22 B. Soula, A. M. Galibert, B. Donnadieu and P.-L. Fabre, *Inorg. Chim. Acta*, 2001, **324**, 90.
23 C. Pena, A. M. Galibert, B. Soula, P.-L. Fabre, G. Bernardinelli and P. Castan, *J. Chem. Soc., Dalton Trans.*, 1998, 239; P. L. Fabre, C. Pena, A. M. Galibert, B. Soula, G. Bernardinelli, B. Donnadieu and P. Castan, *Can. J. Chem.*, 2000, **78**, 280.
24 D. Ranchet, J.-B. Tommasino, O. Vittori and P.-L. Fabre, *J. Solution Chem.*, 1998, **27**, 979.
25 A. M. Bond, E. A. Mc Lennan, R. S. Stojanovic and F. G. Thomas, *Anal. Chem.*, 1987, **59**, 2853.
26 P. Cassoux, R. Dartiguepeyron, C. David, D. de Montauzon, J.-B. Tommasino and P.-L. Fabre, *Actual. Chim.*, 1994, 49 and references therein.
27 Stoe and Cie IPDS Manual, version 2.75 Stoe and Cie, Darmstadt, Germany, 1996.
28 A. Altomare, G. Cascarano, G. Giacovazzo, A. Guagliardi, M. C. Burla, G. Polidori and M. Camalli, *J. Appl. Crystallogr.*, 1994, **27**, 435.
29 G. M. Sheldrick, SHELXL 97, program for the refinement of crystal structures, University of Göttingen, Germany, 1997.
30 WinGX, version 1.63, an integrated system of Windows programs for the solution, refinement and analysis of single crystal X-ray diffraction data: L. J. Farrugia, *J. Appl. Crystallogr.*, 1999, **32**, 837.
31 *International tables for X-ray crystallography*, Kynoch Press, Birmingham, UK, 1974, vol. 4.
32 L. Zolnaï, XPMA, ZORTEP, Graphical programs for X-ray structures analysis, University of Heilderberg, Germany, 1998.
33 B. J. Hathaway, N. Ray, D. Kennedy, N. O'Brien and B. Murphy, *Acta Crystallogr., Sect. B*, 1980, **36**, 1371; F. Clifford, E. Counihan, W. Fitzgerald, K. Seff, C. Simmons, S. Tyagi and B. Hathaway, *J. Chem. Soc., Chem. Commun.*, 1982, 196.
34 I. M. Procter and F. S. Stephens, *J. Chem. Soc. A*, 1969, 1248.
35 H. Zhao, R. A. Heintz, X. Ouyang, K. R. Dunbar, C. F. Campana and R. D. Rogers, *Chem. Mater.*, 1999, **11**, 736.
36 L. Shields, *J. Chem. Soc., Faraday Trans.*, 1985, **2**, 1.
37 C. J. O'Connor, *Prog. Inorg. Chem.*, 1982, **29**, 203.
38 W. Hiller, J. Strähle, A. Datz, M. Hanack, W. E. Hatfield, L. W. ter Haar and P. Gütlich, *J. Am. Chem. Soc.*, 1984, **106**, 329.
39 B. F. Abrahams, K. D. Lu, B. Moubaraki, K. S. Murray and R. Robson, *J. Chem. Soc., Dalton Trans.*, 2000, 1793.
40 B. S. Snyder, G. S. Patterson, A. J. Abrahamson and R. H. Holm, *J. Am. Chem. Soc.*, 1989, **111**, 5214.
41 A. Stassinopoulos, G. Schulte, G. C. Papaefthymiou and J. P. Caradonna, *J. Am. Chem. Soc.*, 1991, **113**, 8686.
42 S. C. Davies, D. L. Hughes, G. J. Leigh, J. R. Sanders and J. S de Souza, *J. Chem. Soc., Dalton Trans.*, 1997, 1981.
43 P.-L. Fabre, F. Dumestre, B. Soula and A. M. Galibert, *Electrochim. Acta*, 2000, **45**, 2697.
44 B. Trémillon, *Electrochimie analytique et réactions en solution, tome 2*, Masson, Paris, 1993.
45 S. A. Richert, P. K. S. Tsang and D. T. Sawyer, *Inorg. Chem.*, 1989, **28**, 2471.
46 M. N. Collomb Dunand-Sauthier, A. Deronzier, C. Duboc Toia, M. Fontecave, K. Gorgy, J.-C. Leprêtre and S. Ménage, *J. Electroanal. Chem.*, 1999, **469**, 53.